Nonadiabatic Photodynamics of Retinal Protonated Schiff base in Channelrhodopsin 2

Ruibin Liang[#†], Fang Liu[#†] and Todd J. Martínez[#†*]

[†] Department of Chemistry and The PULSE Institute, Stanford University, Stanford, CA 94305, USA

[#] SLAC National Accelerator Laboratory, 2575 Sand Hill Road, Menlo Park, CA 94025, USA

* Corresponding Author

Abstract

Channelrhodopsin 2 (ChR2) is a light-gated ion channel and an important tool in optogenetics. Photoisomerization of retinal protonated Schiff base (RPSB) in ChR2 triggers channel activation. Despite the importance of ChR2 in optogenetics, the detailed mechanism for photoisomerization and channel activation is still not fully understood. Here, we report on computer simulations to investigate the photoisomerization mechanism and its effect on the activation of ChR2. Nonadiabatic dynamics simulation of ChR2 was carried out using the *ab initio* multiple spawning (AIMS) method and QM/MM with a restricted ensemble Kohn-Sham (REKS) treatment of the QM region. Our results agree well with spectroscopic measurements, and reveal that the RPSB isomerization is highly specific around the C_{13}=C_{14} bond and follows the "aborted bicycle-pedal" mechanism. In addition, RPSB photoisomerization facilitates its deprotonation and partially increases the hydration level in the channel, which could trigger subsequent channel opening and ion conduction.

Table of Content Graphic

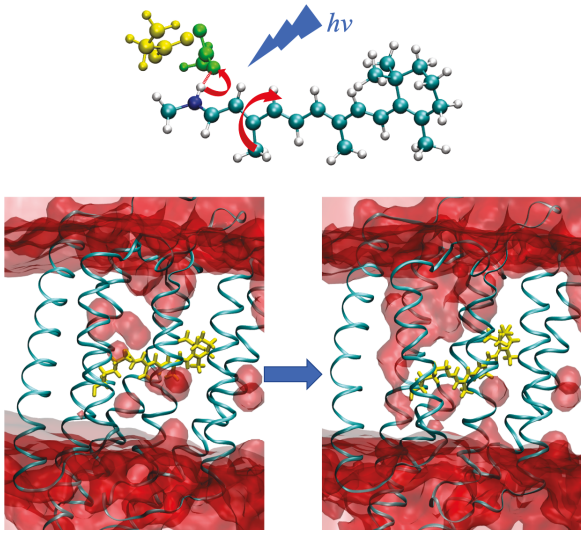

Channelrhodopsin 2 (ChR2) is a light-gated transmembrane cation channel found in the eyespot of motile green algae,[1-4] and is currently the most widely used tool for membrane depolarization in optogenetics.[5] In the photocycle of ChR2, the first intermediate state P500 is reached from the dark state D480 by an essential step where an all-*trans* retinal protonated Schiff base (RPSB, Figures 1B-C) undergoes ultrafast (~400 fs) isomerization around the C_{13}=C_{14} double bond following light excitation, and is converted to the 13-*cis* isomer.[6] Understanding the mechanism of RPSB photoisomerization and its role in channel activation of ChR2 is an important prerequisite for improving the design of optogenetic tools. The crystal structure of a channelrhodopsin chimera formed between ChR1 and ChR2 (C1C2)[7] has stimulated many simulation studies of channelrhodopsin.[8-16] However, in a very recent study, the crystal structure of ChR2 was reported for the first time,[17] and it exhibits several important structural differences in both the channel region and the RPSB chromophore pocket compared to the C1C2 structure.[17] This new ChR2 structure thus calls into question previous hypotheses for the light-activation mechanism, which were based on C1C2-derived homology models of ChR2.[8-13,18] Furthermore, previous simulations of ChR2 did not simulate the non-adiabatic molecular dynamics of RPSB photoisomerization, such that there has been no previous computational study providing a quantitative description of the non-adiabatic dynamics involved in this key reaction step.

The challenging aspects of using non-adiabatic molecular dynamics simulation to investigate RPSB photoisomerization in ChR2 are twofold. Firstly, most electronic structure methods that can correctly describe the excited and ground states of the RPSB are too computationally intensive for *ab initio* molecular dynamics (AIMD) simulation. Secondly, an accurate description of the non-adiabatic dynamics requires accurate solution of the time-dependent Schrödinger equation. Ideally, this entails propagation of nuclear wave-packets on

multiple electronic states, which makes it even more expensive when coupled with on the fly *ab initio* calculation of the potential energy surface (PES).

To overcome the above-mentioned challenges, we integrated state-of-the-art simulation methodologies and the most up-to-date structural information of ChR2 in this work. First, the new ChR2 crystal structure[17] was used as the starting structure in our simulation. Second, we employed full multiple spawning method (FMS)[19-21] to efficiently and accurately solve the time-dependent Schrödinger equation in the non-adiabatic molecular dynamics simulation. Third, during the FMS simulation, the electronic structure of RPSB was treated with the state-interaction state-average spin-restricted ensemble Kohn-Sham method (SI-SA-REKS) method.[22-25] This method accurately and efficiently includes both static and dynamic electron correlation effects that are essential to correctly describe the RPSB isomerization. The accuracy of SI-SA-REKS for isolated RPSB models has been shown previously[26-27] and is further demonstrated in Figure S1, which compares potential energy curves obtained for RPSB torsion in ChR2 with benchmark multireference perturbation theory.[28-29] Graphical processing unit (GPU) acceleration was employed to significantly speed up the SI-SA-REKS calculation.[25,30-31] In addition, ground state QM/MM free energy simulation and microsecond timescale MD classical simulation were carried out to investigate the effect of RPSB isomerization on the activation of ChR2. Our results provide a quantitative description of the non-adiabatic dynamics of the RPSB photoisomerization in ChR2, and provide insight into how this photochemical reaction triggers subsequent channel opening and ion conduction.

The employed computational methodologies are reported in the Supporting Information (SI), and are only briefly summarized here. The protein structure of the transmembrane domain of the ChR2 homo-dimer was taken from the ChR2 crystal structure[17] (PDB code: 6EID), embedded in

the 1-palmitoyl-2-oleoyl-sn-glycero-3-phosphocholine (POPC) lipid bilayer, and solvated by water molecules. In order to prepare starting structures for FMS simulation, 200 ns classical molecular dynamics (MD) equilibration simulations were first performed in the constant NPT ensemble at 300K and 1atm (Figure 1A). Sixty snapshots at 1ns time intervals were taken from the later times of the equilibration trajectory. For each of these snapshots, the system size was reduced to only include the ChR2 protein dimer, the water molecules and ions within 10 Å of the protein, as well as the POPC lipid molecules within 5 Å of the protein. The reduced system was then equilibrated for 2ps with QM/MM MD. The initial conditions (ICs) for the FMS simulations were taken as the final configurations from these ground state QM/MM MD simulations. For each IC, one trajectory basis function (TBF) was placed on S_1 and propagated according to the FMS equations of motion. The PES, gradients and non-adiabatic couplings for S_1 and S_0 were calculated using QM/MM as needed during the FMS simulation, i.e. "on the fly." The QM atoms include the entire RPSB, the $C_\varepsilon H_2$ atoms of Lys257, and the side chains of E123 and D253 in one of the two monomers (Figures 1B-C, total of 68 QM atoms), and were treated with SI-SA-REKS(2,2)[22-25] using the ωPBEh functional[32] and 6-31G basis set. All remaining atoms were modeled with MM using the Amber14 and SPC/Fw classical force fields.[33-37] The FMS simulations (1 ps for each of the 60 ICs) were performed using FMS90 interfaced with the TERACHEM/OPENMM software packages.[30-31,38] In total, our simulations encompass more than 500 ps of QM/MM dynamics for the ChR2 system.

To investigate the effect of RPSB photoisomerization on deprotonation, we performed ground state QM/MM umbrella sampling simulation using the deprotonation coordinate as the collective variable (Figure 4A) for both all-*trans* and 13-*cis* RPSB. Distributions of collective variables were unbiased using WHAM[39] to obtain the RPSB deprotonation free energy profiles.

To further explore the hypothesis that RPSB photoisomerization and deprotonation triggers channel opening, we performed two ~1 μs classical MD simulations starting with different initial conditions. The first one has all-*trans* protonated RPSB and a deprotonated D253 residue in both monomers of ChR2. The second one has 13-*cis* deprotonated RPSB and a protonated D253 residue in one of the two monomers, and all-*trans* protonated RPSB and a deprotonated D253 residue in the other monomer.

RPSB photoisomerization in ChR2. The time evolution of the S_1 population after photoexcitation is shown in Figure 2A. Ground state equilibration dynamics revealed that the RPSB chromophore can be hydrogen bonded to either the E123 or D253 residues. We find that the excited state lifetime is only weakly dependent on which of these residues forms the hydrogen bonded counterion for RPSB. As shown in Figure 2A, the excited state lifetime agrees well with the experimental value (~400 fs).[6] The simulated transient fluorescence spectrum (Figures 2B-C), Stokes' shift (Figure S2A) and D480-P500 absorption difference spectra (Figure S2B) are all in good agreement with the experimental results.[6] The close agreement between simulated and experimental spectra validates both the electronic structure and nonadiabatic dynamics methods we have used.

The protein environment of ChR2 plays a significant role in the RPSB photoisomerization mechanism. The decay time of RPSB in ChR2 is faster than that for RPSB solvated in methanol[40] (2-10 ps), demonstrating that the protein environment surrounding RPSB greatly accelerates its non-adiabatic transition relative to methanol solvent. As shown in Figures 3A-3B, the S_1 population is transferred to S_0 exclusively through the vicinity of the conical intersection (CI) accessed by the rotation about the C_{13}=C_{14} double bond. This highly specific photoisomerization of RPSB in ChR2 contrasts with RPSB solvated in methanol, where the S_1

population is transferred to S_0 through multiple CIs accessed by torsional rotation around multiple double bonds, including C_{13}=C_{14}, C_{11}=C_{12} and C_9=C_{10}.[40] The highly specific RPSB isomerization in ChR2 results, at least partly, from the confinement imposed by the protein environment. In particular, the bulky side chains of the F226, W124, W223 and C128 residues surrounding RPSB largely restrict its motion and enforce specific isomerization around only the C_{13}=C_{14} double bond. It is also evident from Figures 3A-3B that the hydrogen bond acceptors of RPSB (i.e. the counterions) control the direction of the C_{13}=C_{14} bond isomerization. When RPSB is hydrogen bonded to E123, the C_{13}=C_{14} bond rotates in the opposite direction as compared to ICs where RPSB is hydrogen bonded to D253. As a result, two different CIs were approached during photoisomerization. However, the photoisomerization quantum yields (0.61±0.08/0.64±0.07 for ICs with RPSB hydrogen-bonded to E123/D253, respectively) are not strongly dependent on the counterion that is hydrogen bonded to RPSB. To our knowledge, there is currently no reported experimental measurement of the quantum yield for ChR2. Although our quantum yields differ from the measured value for C1C2 (~0.3),[14] they are similar to the measured values for bacteriorhodopsin (~0.6)[41-42] and ChR1 (~0.6).[43]

Our findings contradict those of Guo et al,[15] who concluded that the photoisomerization is more favorable when the RPSB is hydrogen bonded with the E123 residue than with other counterions. The differences between our conclusions may arise from the differences in the system setup (homology model vs. crystal structure), the QM method employed (MS-CASPT2[44] vs. REKS), as well as inclusion of dynamic effects (there is no non-adiabatic dynamics simulation in ref [15]). In addition, we note that the S_2 state is currently not included in our simulation. However, in a recent paper by Dokukina et al,[16] it was found that the S_2 state population rapidly decays to zero after ~100 fs for RPSB photoisomerization in C1C2.[16]

Therefore, we expect that including the S_2 state in our calculation will not significantly slow down the photoisomerization in ChR2.

A closer inspection of the FMS trajectories reveals the detailed motion of RPSB during photoisomerization. After photoexcitation, the backbone C_{14}=C_{13} dihedral angle rotates on the S_1 surface towards the twisted CI, while the backbone N_ζ=C_{15} dihedral angle rotates in the opposite direction (towards planarization), as shown in Figure S3A. After spawning to S_0, the TBFs branch out and eventually reach either the 13-*cis* or the 13-*trans* configurations. For the TBFs which eventually end up in the 13-*cis* configuration, the backbone C_{14}=C_{13} and N_ζ=C_{15} dihedral angles keep rotating in opposite directions until ~ 40 fs after spawning (Figure S3B). At this time, the backbone C_{14}=C_{13} dihedral has almost completed isomerization to 13-*cis*, while the backbone N_ζ=C_{15} dihedral has rotated halfway towards the 90° torsion where a CI is expected. If the backbone N_ζ=C_{15} dihedral mode continued its motion in the same direction, it would lead to thermal isomerization of the N_ζ=C_{15} double bond on S_0, and some TBFs would end up in the 15-*syn*, 13-*cis* configuration. This is not observed, however, because ~ 40-50 fs after the spawning event, the backbone N_ζ=C_{15} dihedral reverses its rotation and moves backwards to the 15-*anti* configuration, while the backbone C_{14}=C_{13} dihedral remains in the 13-*cis* configuration (Figure S3B). As a result, no 15-*syn*, 13-*cis* isomer is formed and the 15-*anti*, 13-*cis* isomer is the only 13-*cis* photoisomerization product in our FMS simulation, in agreement with a recent solid state NMR study of ChR2.[45] Our results are strongly reminiscent of the so-called "aborted bicycle pedal" mechanism (Figure S3C) that has previously been observed in 11-*cis*→all-*trans* RPSB isomerization in rhodopsin.[46] We note that in a recent study of C1C2 by Dokukina et al,[16] the "full bicycle-pedal" mechanism leads to the 13-*cis*, 15-*syn* photoproduct, while the "hula-twist" mechanism leads to the 13-*cis*, 15-*anti* photoproduct.[16] We attribute the differences in our

findings to the differences in the system setup (ChR2 vs. C1C2), the QM method (REKS vs. OM3-MRCI[47-49]), as well as the non-adiabatic dynamic method (AIMS vs. surface hopping[50-51]). During the review of our manuscript, Kuhne et al. reported observing the formation of the 13-*cis*, 15-*syn* photoproduct in parallel with the 13-*cis*, 15-*anti* photoproduct.[52] However, the FTIR signals for this photoproduct were not time-resolved below the nanosecond timescale, making it unclear if the N_ζ=C_{15} isomerization occurs within the ~1 ps time window of our simulation. Therefore, further studies are still necessary to investigate the mechanism of the N_ζ=C_{15} bond isomerization.

The configuration of the photoproduct has further implications for the subsequent deprotonation event. It was found that the 13-*cis, 15-anti* RPSB remains hydrogen bonded to the D253/E123 through the N-H group on the Schiff base, facilitating proton transfer to the counterions.

Effect of isomerization on RPSB deprotonation and hydration increase in ChR2. A central question regarding the ChR2 light-activation mechanism is how RPSB isomerization leads to protein structural changes and channel opening. To answer this question, we employed QM/MM umbrella sampling to calculate the free energy profile (i.e. potential of mean force, PMF) for proton transfer (PT) from RPSB to D253/E123 in both all-trans and 13-cis configurations (Figures 4B/S4, respectively). We find that the PT PMF of 13-cis RPSB has a metastable free energy minimum for protonation of either D253 or E123 (~0.5/1.5 kcal/mol above the free energy minimum for protonated RPSB, respectively). In contrast, for all-trans RPSB, we did not find a free energy minimum for protonated E123 (Figure S4) and the free energy minimum for protonated D253 is 2.5 kcal/mol above the free energy minimum for protonated RPSB (Figure 4B). Therefore, isomerization of RPSB facilitates proton transfer from RPSB to either

D253/E123, with D253 being the most favored of the two proton acceptors. Deprotonation of RPSB was previously shown to be necessary for channel activation during the photocycle of the ChR2.[10] Our results shed light on the results of a previous mutagenesis study, where the E123T mutant preserves the channel activity of ChR2, whereas the the D253N mutant does not.[53] We note that the free energy profile of RPSB deprotonation in C1C2 was recently reported by Adam et al, and the stability of the protonated, all-trans RPSB was also observed.[54]

To further explore the hypothesis that RPSB photoisomerization triggers channel opening, we performed two ~1 μs classical MD simulations of the ChR2 homodimer, with one of the two monomers having all-*trans* protonated RPSB and the other having 13-*cis* deprotonated RPSB with D253 protonated. We find that the hydration level in the channel region increases significantly for the ChR2 monomer with 13-*cis* deprotonated RPSB after ~1 μs. In contrast, the channel remains dehydrated for the ChR2 monomer with all-*trans* protonated RPSB (Figures 4C-D, Figure S5). In other words, the RPSB photoisomerization and deprotonation increases the hydration level in the channel region of the ChR2. However, the channel region is not fully hydrated in our simulation, as there are no continuous water chains throughout the channel (Figure 4D). The lack of continuous water chains prevents cation transport across the channel, indicating that the channel is not yet fully activated for ion conduction. Further protein conformational changes are likely required to fully hydrate and activate the channel. These results agree with previous transient infrared spectroscopic measurements showing that the channel region is only partially hydrated after ~10 μs of photoexcitation, with full hydration occurring ~200 μs after photoexcitation.[55]

Our results can be contrasted with a previous computational study[10] which proposed that RPSB isomerization leads to the breaking of the hydrogen bonds between the E90 and N258

residues, thereby opening the channel. In the simulation of Ref. [10], continuous water chains were formed throughout the channel within ~1μs of RPSB isomerization, which is much faster than the experimentally measured time constant of ~200 μs for full channel hydration. The differences between our simulation results and these previous results are likely a consequence of the different protein structures. The simulation of Ref. [10] was based on a C1C2-derived homology model of ChR2,[7] where the E90 residue is hydrogen bonded to N258 in the dark state. In contrast, our simulation is based on the ChR2 crystal structure,[17] where the E90 residue adopts a different conformation and is not hydrogen bonded to N258 in the dark state. The lack of a hydrogen bond between E90 and N258 in ChR2 before the RPSB photoisomerization explains why the flipping of E90 after the isomerization, which was observed in Ref. [10], is absent in our simulation. Also, the protein cavities on the extracellular side of RPSB are much less hydrated in ChR2 compared to the C1C2 structure, because several salt bridges separate the water clusters in the protein cavities. These salt bridges (which are mostly absent in the C1C2 dark state structure) need to be broken in the process of channel opening as previously proposed.[17] For example, the salt bridges around the R120 residue and the ones near the R268 residue were identified to be essential for the channel gating mechanism.[17] In our simulation, these salt bridges remain intact even after 1μs simulation, regardless of the RPSB configuration and protonation state. This explains why channel hydration increases much faster and to a higher degree after RPSB isomerization in the simulation of Ref. [10] compared to our simulation. Clearly, compared to the simulation of Ref. [10], our simulation better reproduces the structural features observed in the new ChR2 crystal structure.[17] Furthermore, our simulations are in good agreement with transient infrared spectroscopic measurements.[55] Thus, there is reason to believe that our simulation results provide a more accurate rendition of the channel opening mechanism in ChR2. The

simulations of Ref. [10] are more appropriate for the C1C2 chimera, where there is much less experimental data for comparison.

In conclusion, we simulated the photoisomerization of RPSB in ChR2. Our calculated time constant for the $S_1 \rightarrow S_0$ nonadiabatic transition agrees well with experimental measurements. The ChR2 protein environment makes RPSB photoisomerization highly specific around only the $C_{13}=C_{14}$ double bond, and the isomerization follows the "aborted bicycle-pedal" mechanism. The hydrogen bond acceptor of RPSB chromophore, i.e. the D253 or E123 residue, affects the directionality of isomerization, in agreement with a recent simulation of RPSB photoisomerization in C1C2.[16] The two hydrogen bond acceptors have similar effects on the excited state lifetime and quantum yield. Finally, we also conclude that RPSB photoisomerization facilitates its deprotonation (most likely through proton transfer to D253, although proton transfer to E123 is also possible) and partially increases channel hydration, which may eventually lead to full channel opening and ion conduction in ChR2.

Associated Contents

Supporting Information available free of charge on the ACS Publications website.

Computational details for methodology, benchmark electronic structure calculation, absorption and fluorescence spectra, the aborted bicycle-pedal mechanism, the PMF for RPSB deprotonation to E123, and the hydration increase in the channel after RPSB isomerization.

Acknowledgments

This work was supported by the Center for Quantum Molecular Design (CQMD) through the National Science Foundation (CHE-1740645).

References

1. Nagel, G.; Ollig, D.; Fuhrmann, M.; Kateriya, S.; Musti, A. M.; Bamberg, E.; Hegemann, P., Channelrhodopsin-1: A Light-Gated Proton Channel in Green Algae. *Science* **2002,** *296*, 2395.
2. Nagel, G.; Szellas, T.; Huhn, W.; Kateriya, S.; Adeishvili, N.; Berthold, P.; Ollig, D.; Hegemann, P.; Bamberg, E., Channelrhodopsin-2, a directly light-gated cation-selective membrane channel. *Proc. Natl. Acad. Sci. U. S. A.* **2003,** *100*, 13940.
3. Sineshchekov, O. A.; Jung, K.-H.; Spudich, J. L., Two rhodopsins mediate phototaxis to low- and high-intensity light in Chlamydomonas reinhardtii. *Proc. Natl. Acad. Sci. U. S. A.* **2002,** *99*, 8689.
4. Suzuki, T.; Yamasaki, K.; Fujita, S.; Oda, K.; Iseki, M.; Yoshida, K.; Watanabe, M.; Daiyasu, H.; Toh, H.; Asamizu, E.; Tabata, S.; Miura, K.; Fukuzawa, H.; Nakamura, S.; Takahashi, T., Archaeal-type rhodopsins in Chlamydomonas: model structure and intracellular localization. *Biochem. Biophys. Res. Commun.* **2003,** *301*, 711.
5. Schneider, F.; Grimm, C.; Hegemann, P., Biophysics of Channelrhodopsin. *Ann. Rev. Biophys.* **2015,** *44*, 167.
6. Verhoefen, M.-K.; Bamann, C.; Blöcher, R.; Förster, U.; Bamberg, E.; Wachtveitl, J., The Photocycle of Channelrhodopsin-2: Ultrafast Reaction Dynamics and Subsequent Reaction Steps. *Chemphyschem* **2010,** *11*, 3113.
7. Kato, H. E.; Zhang, F.; Yizhar, O.; Ramakrishnan, C.; Nishizawa, T.; Hirata, K.; Ito, J.; Aita, Y.; Tsukazaki, T.; Hayashi, S.; Hegemann, P.; Maturana, A. D.; Ishitani, R.; Deisseroth, K.; Nureki, O., Crystal structure of the channelrhodopsin light-gated cation channel. *Nature* **2012,** *482*, 369.
8. Watanabe, H. C.; Welke, K.; Sindhikara, D. J.; Hegemann, P.; Elstner, M., Towards an Understanding of Channelrhodopsin Function: Simulations Lead to Novel Insights of the Channel Mechanism. *J. Mol. Biol.* **2013,** *425*, 1795.
9. Dokukina, I.; Weingart, O., Spectral properties and isomerisation path of retinal in C1C2 channelrhodopsin. *Phys. Chem. Chem. Phys.* **2015,** *17*, 25142.
10. Kuhne, J.; Eisenhauer, K.; Ritter, E.; Hegemann, P.; Gerwert, K.; Bartl, F., Early Formation of the Ion-Conducting Pore in Channelrhodopsin-2. *Ang. Chem. Int. Ed.* **2015,** *54*, 4953.
11. Takemoto, M.; Kato, H. E.; Koyama, M.; Ito, J.; Kamiya, M.; Hayashi, S.; Maturana, A. D.; Deisseroth, K.; Ishitani, R.; Nureki, O., Molecular Dynamics of Channelrhodopsin at the Early Stages of Channel Opening. *PLoS One* **2015,** *10*, e0131094.
12. Guo, Y.; Beyle, F. E.; Bold, B. M.; Watanabe, H. C.; Koslowski, A.; Thiel, W.; Hegemann, P.; Marazzi, M.; Elstner, M., Active site structure and absorption spectrum of channelrhodopsin-2 wild-type and C128T mutant. *Chem. Sci.* **2016,** *7*, 3879.
13. VanGordon, M. R.; Gyawali, G.; Rick, S. W.; Rempe, S. B., Atomistic Study of Intramolecular Interactions in the Closed-State Channelrhodopsin Chimera, C1C2. *Biophys. J.* **2017,** *112*, 943.
14. Hontani, Y.; Marazzi, M.; Stehfest, K.; Mathes, T.; van Stokkum, I. H. M.; Elstner, M.; Hegemann, P.; Kennis, J. T. M., Reaction dynamics of the chimeric channelrhodopsin C1C2. *Sci. Rep.* **2017,** *7*, 7217.
15. Guo, Y.; Wolff, F. E.; Schapiro, I.; Elstner, M.; Marazzi, M., Different hydrogen bonding environments of the retinal protonated Schiff base control the photoisomerization in channelrhodopsin-2. *Phys. Chem. Chem. Phys.* **2018,** *20*, 27501.

16. Dokukina, I.; Nenov, A.; Garavelli, M.; Marian, C. M.; Weingart, O., QM/MM Photodynamics of Retinal in the Channelrhodopsin Chimera C1C2 with OM3/MRCI. *ChemPhotoChem* **2019,** *3*, 107.
17. Volkov, O.; Kovalev, K.; Polovinkin, V.; Borshchevskiy, V.; Bamann, C.; Astashkin, R.; Marin, E.; Popov, A.; Balandin, T.; Willbold, D.; Büldt, G.; Bamberg, E.; Gordeliy, V., Structural insights into ion conduction by channelrhodopsin 2. *Science* **2017,** *358*.
18. Ardevol, A.; Hummer, G., Retinal isomerization and water-pore formation in channelrhodopsin-2. *Proc. Natl. Acad. Sci. U. S. A.* **2018,** *115*, 3557.
19. Ben-Nun, M.; Martínez, T. J., Nonadiabatic molecular dynamics: Validation of the multiple spawning method for a multidimensional problem. *J. Chem. Phys.* **1998,** *108*, 7244.
20. Ben-Nun, M.; Quenneville, J.; Martínez, T. J., Ab Initio Multiple Spawning: Photochemistry from First Principles Quantum Molecular Dynamics. *J. Phys. Chem. A* **2000,** *104*, 5161.
21. Ben-Nun, M.; Martínez, T. J., Ab Initio Quantum Molecular Dynamics. *Adv. Chem. Phys.* **2002,** *121*, 439.
22. Filatov, M., Spin-restricted ensemble-referenced Kohn–Sham method: basic principles and application to strongly correlated ground and excited states of molecules. *WIRes: Comp. Mol. Sci.* **2015,** *5*, 146.
23. Filatov, M.; Liu, F.; Martinez, T. J., Analytical derivatives of the individual state energies in ensemble density functional theory method. I. General formalism. *J. Chem. Phys.* **2017,** *147*, 034113.
24. Filatov, M.; Liu, F.; Kim, K. S.; Martinez, T. J., Self-consistent implementation of ensemble density functional theory method for multiple strongly correlated electron pairs. *J. Chem. Phys.* **2016,** *145*, 244104.
25. Liu, F.; Filatov, M.; Martínez, T. J. Analytical Derivatives of the Individual State Energies in Ensemble Density Functional Theory Method: II. Implementation on Graphical Processing Units (GPUs) *ChemRxiv* [Online], 2019. https://doi.org/10.26434/chemrxiv.7985657.v1
26. Huix-Rotllant, M.; Filatov, M.; Gozem, S.; Schapiro, I.; Olivucci, M.; Ferré, N., Assessment of Density Functional Theory for Describing the Correlation Effects on the Ground and Excited State Potential Energy Surfaces of a Retinal Chromophore Model. *J. Chem. Theory Comput.* **2013,** *9*, 3917.
27. Filatov, M.; Min, S. K.; Kim, K. S., Direct Nonadiabatic Dynamics by Mixed Quantum-Classical Formalism Connected with Ensemble Density Functional Theory Method: Application to trans-Penta-2,4-dieniminium Cation. *J. Chem. Theory Comput.* **2018,** *14*, 4499.
28. Roos, B. O., Theoretical Studies of Electronically Excited States of Molecular Systems Using Multiconfigurational Perturbation Theory. *Acc. Chem. Res.* **1999,** *32*, 137.
29. Gozem, S.; Melaccio, F.; Lindh, R.; Krylov, A. I.; Granovsky, A. A.; Angeli, C.; Olivucci, M., Mapping the Excited State Potential Energy Surface of a Retinal Chromophore Model with Multireference and Equation-of-Motion Coupled-Cluster Methods. *J. Chem. Theory Comput.* **2013,** *9*, 4495.
30. Ufimtsev, I. S.; Martinez, T. J., Quantum Chemistry on Graphical Processing Units. 3. Analytical Energy Gradients, Geometry Optimization, and First Principles Molecular Dynamics. *J. Chem. Theory Comput.* **2009,** *5*, 2619.
31. Titov, A. V.; Ufimtsev, I. S.; Luehr, N.; Martinez, T. J., Generating Efficient Quantum Chemistry Codes for Novel Architectures. *J. Chem. Theory Comput.* **2013,** *9*, 213.

32. Rohrdanz, M. A.; Martins, K. M.; Herbert, J. M., A long-range-corrected density functional that performs well for both ground-state properties and time-dependent density functional theory excitation energies, including charge-transfer excited states. *J. Chem. Phys.* **2009,** *130*, 054112.
33. Maier, J. A.; Martinez, C.; Kasavajhala, K.; Wickstrom, L.; Hauser, K. E.; Simmerling, C., ff14SB: Improving the Accuracy of Protein Side Chain and Backbone Parameters from ff99SB. *J. Chem. Theory Comput.* **2015,** *11*, 3696.
34. Wang, J.; Wolf, R. M.; Caldwell, J. W.; Kollman, P. A.; Case, D. A., Development and testing of a general amber force field. *J. Comput. Chem.* **2004,** *25*, 1157.
35. Wang, J.; Wang, W.; Kollman, P. A.; Case, D. A., Automatic atom type and bond type perception in molecular mechanical calculations. *J. Mol. Graph. Model.* **2006,** *25*, 247.
36. Dickson, C. J.; Madej, B. D.; Skjevik, Å. A.; Betz, R. M.; Teigen, K.; Gould, I. R.; Walker, R. C., Lipid14: The Amber Lipid Force Field. *J. Chem. Theory Comput.* **2014,** *10*, 865.
37. Wu, Y. J.; Tepper, H. L.; Voth, G. A., Flexible simple point-charge water model with improved liquid-state properties. *J. Chem. Phys.* **2006,** *124*.
38. Eastman, P.; Friedrichs, M. S.; Chodera, J. D.; Radmer, R. J.; Bruns, C. M.; Ku, J. P.; Beauchamp, K. A.; Lane, T. J.; Wang, L.-P.; Shukla, D.; Tye, T.; Houston, M.; Stich, T.; Klein, C.; Shirts, M. R.; Pande, V. S., OpenMM 4: A Reusable, Extensible, Hardware Independent Library for High Performance Molecular Simulation. *J. Chem. Theory Comput.* **2013,** *9*, 461.
39. Kumar, S.; Bouzida, D.; Swendsen, R. H.; Kollman, P. A.; Rosenberg, J. M., The Weighted Histogram Analysis Method for Free-Energy Calculations on Biomolecules. 1. The Method. *J. Comput. Chem.* **1992,** *13*, 1011.
40. Punwong, C.; Owens, J.; Martinez, T. J., Direct QM/MM Excited-State Dynamics of Retinal Protonated Schiff Base in Isolation and Methanol Solution. *J. Phys. Chem. B* **2015,** *119*, 704.
41. Tittor, J.; Oesterhelt, D., The quantum yield of bacteriorhodopsin. *FEBS Lett.* **1990,** *263*, 269.
42. Logunov, S. L.; El-Sayed, M. A.; Song, L.; Lanyi, J. K., Photoisomerization Quantum Yield and Apparent Energy Content of the K Intermediate in the Photocycles of Bacteriorhodopsin, Its Mutants D85N, R82Q, and D212N, and Deionized Blue Bacteriorhodopsin. *J. Phys. Chem.* **1996,** *100*, 2391.
43. Stensitzki, T.; Yang, Y.; Muders, V.; Schlesinger, R.; Heberle, J.; Heyne, K., Femtosecond infrared spectroscopy of channelrhodopsin-1 chromophore isomerization. *Struct. Dyn.* **2016,** *3*, 043208.
44. Finley, J.; Malmqvist, P.-Å.; Roos, B. O.; Serrano-Andrés, L., The multi-state CASPT2 method. *Chem. Phys. Lett.* **1998,** *288*, 299.
45. Becker-Baldus, J.; Bamann, C.; Saxena, K.; Gustmann, H.; Brown, L. J.; Brown, R. C. D.; Reiter, C.; Bamberg, E.; Wachtveitl, J.; Schwalbe, H.; Glaubitz, C., Enlightening the photoactive site of channelrhodopsin-2 by DNP-enhanced solid-state NMR spectroscopy. *Proc. Natl. Acad. Sci. U. S. A.* **2015,** *112*, 9896.
46. Warshel, A.; Barboy, N., Energy storage and reaction pathways in the first step of the vision process. *J. Am. Chem. Soc.* **1982,** *104*, 1469.
47. Weber, W.; Thiel, W., Orthogonalization corrections for semiempirical methods. *Theor. Chem. Acc.* **2000,** *103*, 495.
48. Fabiano, E.; Keal, T. W.; Thiel, W., Implementation of surface hopping molecular dynamics using semiempirical methods. *Chem. Phys.* **2008,** *349*, 334.

49. Dral, P. O.; Wu, X.; Spörkel, L.; Koslowski, A.; Weber, W.; Steiger, R.; Scholten, M.; Thiel, W., Semiempirical Quantum-Chemical Orthogonalization-Corrected Methods: Theory, Implementation, and Parameters. *J. Chem. Theory Comput.* **2016,** *12*, 1082.
50. Tully, J. C.; Preston, R. K., Trajectory Surface Hopping Approach to Nonadiabatic Molecular Collisions: The Reaction of H with D2. *J. Chem. Phys.* **1971,** *55*, 562.
51. Tully, J. C., Molecular dynamics with electronic transitions. *J. Chem. Phys.* **1990,** *93*, 1061.
52. Kuhne, J.; Vierock, J.; Tennigkeit, S. A.; Dreier, M.-A.; Wietek, J.; Petersen, D.; Gavriljuk, K.; El-Mashtoly, S. F.; Hegemann, P.; Gerwert, K., Unifying photocycle model for light adaptation and temporal evolution of cation conductance in channelrhodopsin-2. *Proc. Natl. Acad. Sci. U. S. A.* **2019,** *116*, 9380.
53. Lórenz-Fonfría, V. A.; Resler, T.; Krause, N.; Nack, M.; Gossing, M.; Fischer von Mollard, G.; Bamann, C.; Bamberg, E.; Schlesinger, R.; Heberle, J., Transient protonation changes in channelrhodopsin-2 and their relevance to channel gating. *Proc. Natl. Acad. Sci. U. S. A.* **2013,** *110*, E1273.
54. Adam, S.; Bondar, A.-N., Mechanism by which water and protein electrostatic interactions control proton transfer at the active site of channelrhodopsin. *PLoS One* **2018,** *13*, e0201298.
55. Lórenz-Fonfría, V. A.; Bamann, C.; Resler, T.; Schlesinger, R.; Bamberg, E.; Heberle, J., Temporal evolution of helix hydration in a light-gated ion channel correlates with ion conductance. *Proc. Natl. Acad. Sci. U. S. A.* **2015,** *112*, E5796.

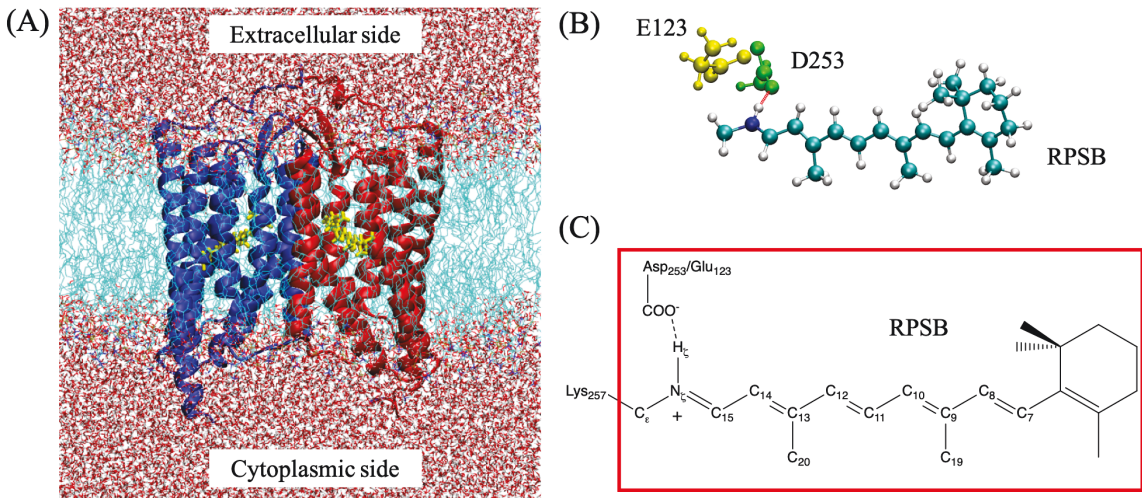

Figure 1. RPSB in channelrhodopsin 2 (ChR2). (A) The equilibrated ChR2 transmembrane domain embedded in POPC lipid bilayer and solvated by water molecules. The protein is shown in new-cartoon style and is colored in red or blue for each monomer. The RPSB molecules are shown in licorice style and colored in yellow. The POPC lipid bilayer and water molecules are colored in green and red, respectively. (B) The QM region of the system, including the RPSB molecule (in cyan), the D253 (in green) and the E123 residues. The red line between NH group of RPSB and the D253 residue indicates the hydrogen bond between them. (C) Chemical formula of the RPSB covalently bonded to the side chain of Lys257. The red frame encircles the atoms in the QM region. The dashed line indicates the hydrogen bond between the deprotonated E123/D253 carboxyl group and the positively charged NH group in the RPSB on the ground state. The atom naming convention in this figure is followed in the main text.

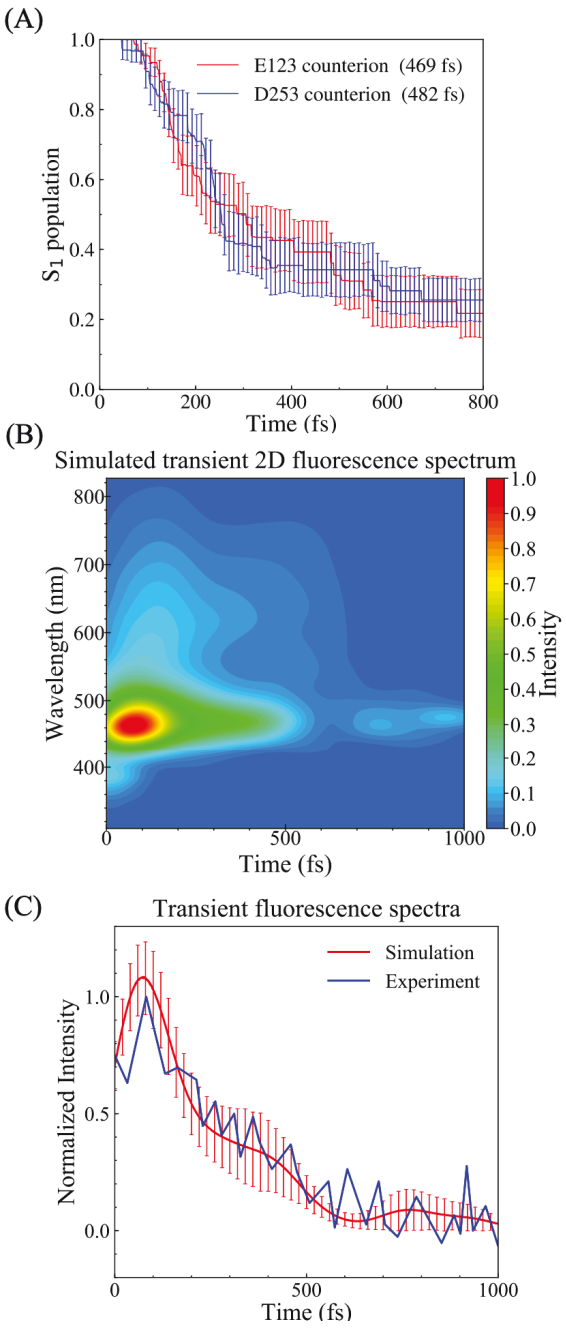

Figure 2. (A) The $S_1 \rightarrow S_0$ population decay in channelrhodopsin 2 from AIMS simulations of photoexcitation from the fully equilibrated ChR2 crystal structure. (B) Simulated 2D transient fluorescence spectrum. (C) 1D transient fluorescence spectrum calculated from simulation (457 nm) and experiment (520 nm, Figure 2D in Ref 6). The shift between simulation and experiment is obtained from the calculation of fluorescence spectra (SI). See SI for the details of spectra calculation.

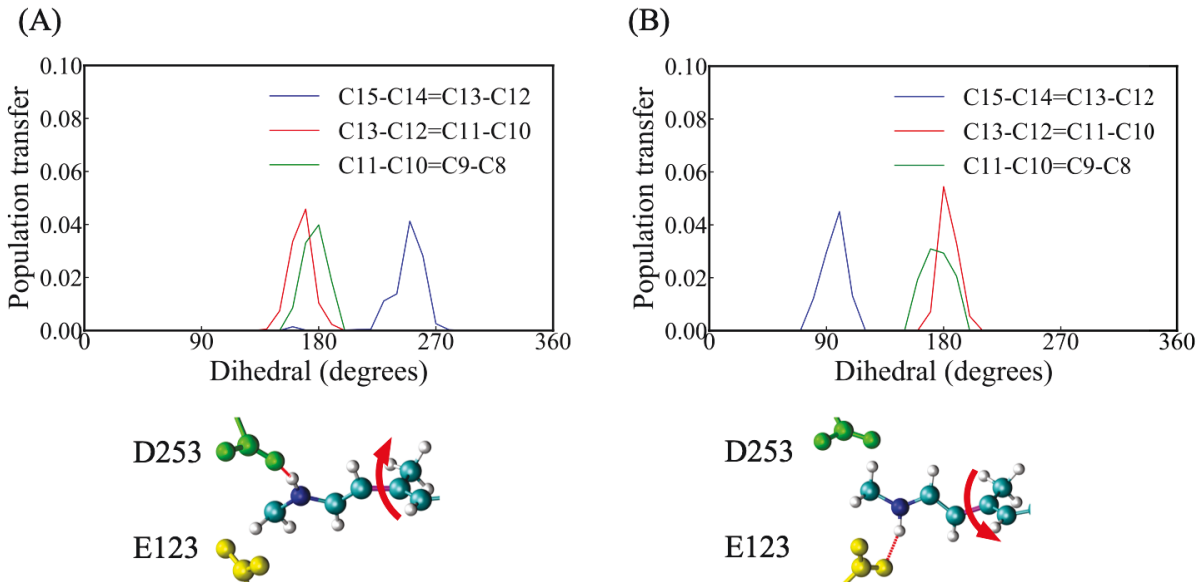

Figure 3. Amount of $S_1 \rightarrow S_0$ population transfer as a function of different torsional reaction coordinates, for initial conditions where either (A) the D253 residue or (B) the E123 residue is the counterion hydrogen bonded to RPSB. The insets indicate the RPSB conformations near the conical intersection where the population transfer occurs. The isomerizing double bond is colored in purple, and the direction of the rotation is indicated by the red arrows. The population transfer is exclusively centered near the CIs accessed by the C_{15}-C_{14}=C_{13}-C_{12} dihedral rotation only, indicating high specificity of isomerization process due to the confinement of surrounding protein environment. Also, the RPSB hydrogen bond acceptor, i.e. the counterion D253 (green) or E123 (yellow), determines the directionality of the isomerization.

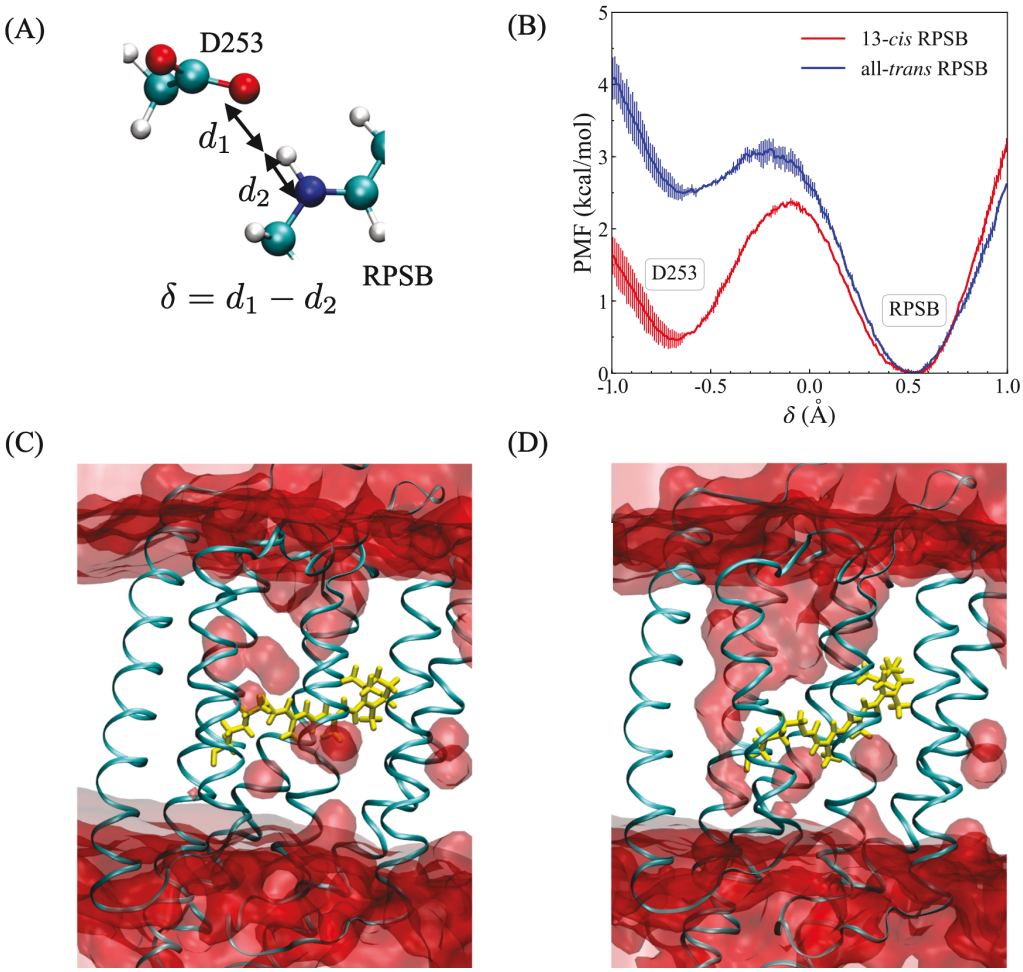

Figure 4. The photoisomerization of RPSB facilitates proton transfer to one of the nearby counterions, and increases the hydration in the channel region of ChR2. (A) The definition of the proton transfer reaction coordinate δ= *d*(Hζ-OD) - *d*(Hζ-Nζ), i.e. the difference between the Hζ-Nζ and Hζ-OD, bond lengths, where OD is the carboxyl oxygen proton acceptor of D253. (B) The free energy profile for RPSB deprotonation before/after (blue/red) RPSB photoisomerization when D253 is the proton acceptor. The free energy wells corresponding to protonated states of RPSB or the counterion are labeled as boxed text. (C)-(D) Water density (red) in one monomer of the ChR2 where the RPSB is in all-*trans* protonated and 13-*cis* deprotonated state, respectively.